J. Mech. Phys. Solids Vol. 40, No. 6, pp. 1377–1397, 1992
Printed in Great Britain

0022-5096/92 $5.00 + 0.00

THE RELATION BETWEEN CRACK GROWTH RESISTANCE AND FRACTURE PROCESS PARAMETERS IN ELASTIC–PLASTIC SOLIDS

VIGGO TVERGAARD
Department of Solid Mechanics, The Technical University of Denmark, DK-2800 Lyngby, Denmark

and

JOHN W. HUTCHINSON
Division of Applied Sciences, Harvard University, Cambridge, MA 02138, U.S.A.

(*Received* 1 *March* 1991)

ABSTRACT

CRACK growth initiation and subsequent resistance is computed for an elastic–plastic solid with an idealized traction–separation law specified on the crack plane to characterize the fracture process. The solid is specified by its Young's modulus, E, Poisson's ratio, ν, initial tensile yield stress, σ_Y, and strain hardening exponent, N. The primary parameters specifying the traction–separation law of the fracture process are the work of separation per unit area, Γ_0, and the peak traction, $\hat{\sigma}$. Highly refined calculations have been carried out for resistance curves, $K_R(\Delta a)$, for plane strain, mode I growth in small-scale yielding as dependent on the parameters characterizing the elastic–plastic properties of the solid and its fracture process. With $K_0 = [E\Gamma_0/(1-\nu^2)]^{1/2}$ as the intensity needed to advance the crack in the absence of plasticity, K_R/K_0 is presented in terms of its dependence on the two most important parameters, $\hat{\sigma}/\sigma_Y$ and N, with special emphasis on initiation toughness and steady-state toughness. Three applications of the results are made: to predict toughnesss when the fracture process is void growth and coalescence, to predict the role of plasticity on interface toughness for similar materials bonded together, and to illuminate the role of plasticity in enhancing toughness in dual-phase solids. The regime of applicability of the present model to ductile fracture due to void growth and coalescence, wherein multiple voids interact within the fracture process zone, is complementary to the regime of applicability of models describing the interaction between a single void and the crack tip. The two mechanism regimes are delineated and the consequence of a transition between them is discussed.

1. INTRODUCTION

SUBTLETIES aside, the Griffith criterion for elastic crack growth is

$$\mathcal{G} = \Gamma_0, \tag{1.1}$$

where Γ_0 is the work of separation per unit area required to create the two crack surfaces and $\mathcal{G}$ is the energy release rate as calculated for a line crack using elasticity theory. In attempting to apply Griffith's approach to metals in the early 1950s, Orowan and Irwin realized that dissipation caused by the high stresses in the plastic zone

surrrounding the crack tip played a major role in the work balance. However, a fundamental relation between the total work of fracture and the work of the fracture process Γ_0 was not to be found. Even today, there are essentially no quantitative results available specifying this relationship for plane strain, mode I crack growth. This is the objective of the present paper. It is motivated by the desire to have a more fundamental understanding of the role of plasticity in contributing to toughness of a wide range of ductile materials. While long experience contributes to this understanding for metals, there is little experience on which judgement can be based for systems such as particulate-reinforced metal–matrix composites and materials joined at an interface where at least one material has some ductility.

The approach which did emerge in the 1960s, largely due to Irwin, was phenomenological. Under conditions of small-scale yielding (and, for definiteness, assume also mode I, plane strain behavior) the criterion for crack advance is taken as

$$\mathcal{G} = \Gamma_R(\Delta a), \tag{1.2}$$

where the crack growth resistance, $\Gamma_R(\Delta a)$, for a particular material under given environmental conditions is to be determined by experiment. The fact that $\Gamma_R(\Delta a)$ usually increases with increasing Δa reflects the fact that the plastic field at the crack changes as the crack advances. Plastic dissipation evidently depends on both Γ_0 and Δa.

This criterion can be restated as an intensity-based condition. With K as the plane strain, mode I stress intensity factor, Irwin's relation,

$$\mathcal{G} = (1-\nu^2)K^2/E, \tag{1.3}$$

permits (1.2) to be written as

$$K = K_R(\Delta a), \tag{1.4}$$

where $K_R = [E\Gamma_R\,(1-\nu^2)]^{1/2}$, ν is Poisson's ratio, and E is Young's modulus. In this paper the concern will be exclusively with small-scale yielding, rate-independent behavior under monotonically increasing K or $\mathcal{G}$. The intensity-based criterion is completely equivalent to the energy equation (1.2) under these circumstances.

A more fundamental approach to crack growth resistance was initiated by McCLINTOCK and IRWIN (1965) who used small-scale yielding solutions for growing cracks in mode III, together with a model propagation criterion based on the attainment of a critical strain at a characteristic distance ahead of the tip. This approach culminated in the work of Rice and coworkers (RICE and SORENSEN, 1978; RICE *et al.*, 1980) on plane strain, mode I. In the mode I work, solutions for the crack opening profile behind the advancing tip were obtained. The refined numerical calculations of SHAM (1983) were used to establish the relation of the opening profile on K and Δa. A propagation criterion was imposed on the solution requiring that the near-tip opening profile be invariant once propagation is under way. The outcome of the approach was the prediction of the crack growth resistance curve, $K_R(\Delta a)$.

The approach adopted in this paper goes one step further than that just described by directly coupling a model of the fracture process to the elastic–plastic field of the growing crack. Plastic dissipation and crack growth resistance are then calculated in terms of the parameters characterizing the fracture process and the continuum prop-

erties of the solid. The fracture process is modeled by a traction–separation boundary condition specified along the crack plane. The approach taken here is similar in many of its aspects to studies by NEEDLEMAN (1987, 1990) on decohesion at interfaces in the presence of plastic deformation.

1.1. *The parameters and implications from dimensional analysis*

The traction–separation relation used to model the fracture process in the present study is shown in Fig. 1. The work of separation per unit area is

$$\Gamma_0 = \int_0^{\delta_c} \sigma \, \mathrm{d}\delta = \tfrac{1}{2}\hat{\sigma}[\delta_c + \delta_2 - \delta_1]. \tag{1.5}$$

This separation law is fully specified by Γ_0, $\hat{\sigma}$, δ_1/δ_c and δ_2/δ_c, where the latter two parameters can be thought of as "shape" parameters.

The elastic–plastic solid has an initial tensile yield stress, σ_Y, and a true stress–logarithmic strain curve in uniaxial tension specified by

$$\begin{aligned} \varepsilon &= \sigma/E && \sigma \leqslant \sigma_Y, \\ &= (\sigma_Y/E)(\sigma/\sigma_Y)^{1/N} && \sigma \geqslant \sigma_Y. \end{aligned} \tag{1.6}$$

The limit of zero strain hardening index, N, corresponds to an elastic–perfectly plastic solid. The tensile behavior is generalized to multiaxial stress states assuming isotropic hardening and using the mises yield surface, as discussed in the next section. Thus, the continuum behavior of the solid is characterized by the set of parameters E, ν, σ_Y and N.

The complete list of parameters characterizing the fracture process and the deformation of the solid is:

$$\Gamma_0, \hat{\sigma}, \delta_1/\delta_c \text{ and } \delta_2/\delta_c \quad \text{(fracture process)}, \tag{1.7a}$$

$$\sigma_Y, N, E \text{ and } \nu \quad \text{(solid)}. \tag{1.7b}$$

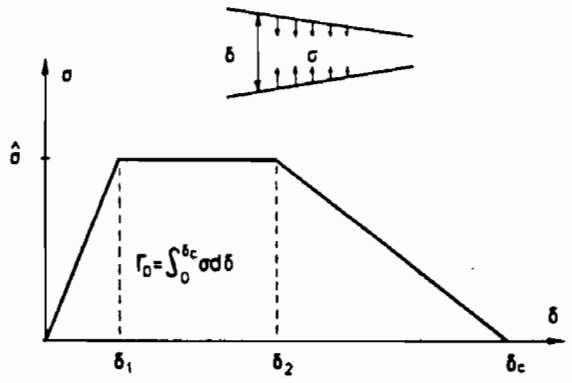

FIG. 1. Traction–separation relation for fracture process.

Two reference quantities will now be defined which will be used to present results. The reference intensity factor

$$K_0 \equiv [E\Gamma_0/(1-\nu^2)]^{1/2} \tag{1.8}$$

is the intensity needed to advance the crack in the absence of plasticity ($\sigma_Y \to \infty$), according to the Griffith criterion (1.1) with (1.3). A reference length is defined by

$$R_0 \equiv \frac{1}{3\pi(1-\nu^2)}\frac{E\Gamma_0}{\sigma_Y^2} = \frac{1}{3\pi}\left(\frac{K_0}{\sigma_Y}\right)^2. \tag{1.9}$$

This reference value scales with the extent of the plastic zone size when $K \cong K_0$. In small-scale yielding, $(K/\sigma_Y)^2/(3\pi)$ is often used as an estimate of the size of the plastic zone.

The results of highly refined calculations will be presented for the resistance curve, $K_R(\Delta a)$, and for the steady-state toughness, $K_R^{ss} = K_R(\Delta a)$ as $\Delta a \to \infty$, together with other quantities of interest. Dimensional analysis reveals that the solution must depend on dimensionless combinations of the parameter set (1.7) in the following way:

$$\frac{K_R(\Delta a)}{K_0} = F\left[\frac{\Delta a}{R_0}, \frac{\dot\sigma}{\sigma_Y}, N, \frac{\sigma_Y}{E}, \nu, \frac{\delta_1}{\delta_c}, \frac{\delta_2}{\delta_c}\right] \tag{1.10}$$

and

$$\frac{K_R^{ss}}{K_0} = F_{ss}\left[\frac{\dot\sigma}{\sigma_Y}, N, \frac{\sigma_Y}{E}, \nu, \frac{\delta_1}{\delta_c}, \frac{\delta_2}{\delta_c}\right], \tag{1.11}$$

where F_{ss} is the limit of F as $\Delta a\ R_0 \to \infty$. Other combinations of the nondimensional parameters could be used, but this particular choice has the advantage that the most important nondimensional parameters are found to be $\dot\sigma\ \sigma_Y$ and N, as well as $\Delta a\ R_0$ for the transient growth behavior. Note that (1.11) is equivalent to

$$\Gamma_R^{ss} = \Gamma_0 F_{ss}^2[\dot\sigma\ \sigma_Y, N, \ldots], \tag{1.12}$$

which follows directly using (1.3) and (1.8). Thus, steady-state toughness, measured as a critical energy release rate, necessarily scales with the work of the fracture process, Γ_0. In a steady state it can be rigorously stated that the total energy release rate, Γ_R^{ss}, equals the work of the fracture process, Γ_0, plus the additional contribution, $\Gamma_0(F_{ss}^2 - 1)$, which is mainly plastic dissipation together with a small amount of elastic energy locked in the crack wake. Thus the numerical results presented later in this paper provide a rigorous partitioning of the total work of fracture into these two contributions when the crack is growing in the steady state. The equivalent statement with respect to transient growth is not correct since the elastic strain energy within and just outside the plastic zone is not constant but changes as the zone size increases and as the wake of plastic strains develops. Only in a steady state is the stress field unchanging for an observer advancing with the tip, and thus only in this limiting condition is the distribution of elastic strain energy density invariant with respect to the advancing tip. In the transient period, which includes initiation, the changing elastic energy distribution makes its own significant contribution to the work balance.

Attempts to identify the parameters of the traction-separation law with characteristics of specific fracture mechanisms will be postponed until Sections 4 and 5. There the results will be applied to a fracture process involving void growth and coalescence under conditions in which multiple interacting voids in a "void-sheet" ahead of the crack tip form the fracture process zone. It will be argued that this situation constitutes a mechanism regime distinct from the situation where most of the interaction is confined to a single void interacting with the crack tip. Predictions for these two regimes will be compared. The basic model is applicable to crack propagation along an interface where two identical solids have been bonded together. In this case, where the parameters of the fracture process describe interface separation, a clear picture emerges as to whether or not plastic dissipation in the adjoining material halves will contribute to the effective interface toughness. In addition, application of the model results will be made to draw qualitative conclusions about the role of plasticity in enhancing toughness of dual-phase solids with one phase much harder than the other.

2. Specification of the Model

The present analyses of plane strain mode I crack growth are carried out for conditions of small-scale yielding. Due to symmetry about the crack plane only half of the solid needs to be analyzed, and the numerical computations are carried out for a semicircular region with initial radius A_0, as shown in Fig. 2. The x^1-axis is in the crack plane and the initial crack tip is located at $x^1 = x^2 = 0$.

The traction–separation relation used to model the fracture process (see Fig. 1) is specified everywhere on the boundary $x^1 > 0$, $x^2 = 0$ of the region analyzed, while zero tractions are specified for $x^1 \leqslant 0$, $x^2 = 0$. On the outer semicircular boundary displacements are specified according to the K-field around the crack tip as the origin. Thus, the loading is applied by incrementally increasing the amplitude K of the displacements on the semicircular boundary.

Finite strains are accounted for in the analysis, and the deformations are taken to be described by J_2 flow theory. A convected-coordinate, Lagrangian formulation of the field equations is used, in which g_{ij} and G_{ij} are metric tensors in the reference configuration and the current configuration, respectively, with determinants g and G, and $\eta_{ij} = \frac{1}{2}(G_{ij} - g_{ij})$ is the Lagrangian strain tensor.

The contravariant components τ^{ij} of the Kirchhoff stress tensor on the current base vectors are related to the components of the Cauchy stress tensor σ^{ij} by $\tau^{ij} = \sqrt{G/g}\,\sigma^{ij}$. Then, in the finite-strain generalization of J_2 flow theory discussed by Hutchinson (1973), the incremental stress–strain relationship is of the form $\dot{\tau}^{ij} = L^{ijkl}\dot{\eta}_{kl}$, with the tensor of instantaneous moduli given by

$$L^{ijkl} = \frac{E}{1+\nu}\left[\frac{1}{2}(G^{ik}G^{jl}+G^{il}G^{jk}) + \frac{\nu}{1-2\nu}G^{ij}G^{kl} - \beta\frac{3/2(E/E_t-1)}{E/E_t-(1-2\nu)/3}\frac{s^{ij}s^{kl}}{\sigma_e^2}\right]$$
$$-\tfrac{1}{2}(G^{ik}\tau^{jl}+G^{jk}\tau^{il}+G^{il}\tau^{jk}+G^{jl}\tau^{ik}) \quad (2.1)$$

where the effective Mises stress is $\sigma_e = (3s_{ij}s^{ij}/2)^{1/2}$, $s^{ij} = \tau^{ij} - G^{ij}\tau^k_k/3$ is the stress

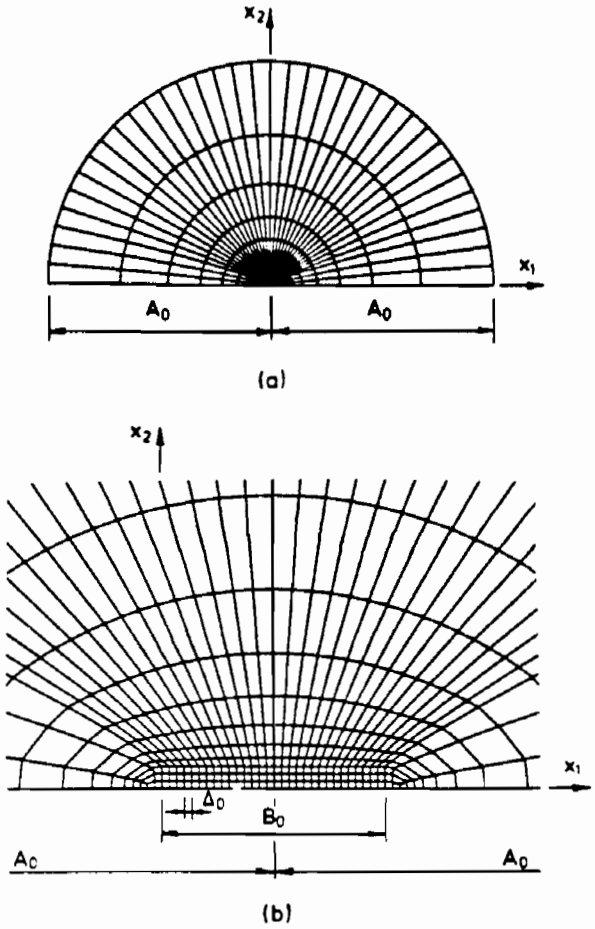

FIG. 2. Finite-element grid. (a) Full grid. (b) Refined grid along crack line.

deviator, and the value of β is 1 or 0 for plastic yielding or elastic unloading, respectively. Furthermore, E is Young's modulus, ν is Poisson's ratio, and E_t is the slope of the true stress vs natural strain curve (1.6) at the stress level σ_e. In the case of an elastic–perfectly plastic material [$N = 0$ in (1.6)] the instantaneous moduli are obtained from (2.1) as the limit $E_t/E = 0$.

It is noted that the stress σ used in the traction–separation relation (Fig. 1) is defined as a true stress. This is important in cases where crack tip blunting starts to occur, since then elements near the crack tip are strongly deformed by finite straining, and the true stress carrying capacity in the interface adjacent to strongly deformed elements would far exceed the assumed maximum value $\hat{\sigma}$ if nominal stresses were applied in the traction–separation relation rather than true stresses. However, in most of the computations to be reported here all strains remain rather small, so that

applying true stresses or nominal stresses in the traction–separation relationship would not make much difference.

The value of the J-integral is calculated on several contours to check agreement with the prescribed amplitude K of the edge displacements. In the finite-strain context the expression for J is (RICE, 1968; ESHELBY, 1970)

$$J = \int_\Gamma [W\,\mathrm{d}x^2 - T^i u_{i,1}\,\mathrm{d}s], \quad W = \int_0^{\eta_{ij}} \tau^{ij}\delta\eta_{ij}. \tag{2.2}$$

where Γ is some path, in the reference configuration, from the lower crack surface to the upper crack surface, $\mathrm{d}s$ is an arc length element along this path, and T^i are the nominal tractions on the boundary of the region enclosed by the contour Γ. As long as the radius A_0 is chosen large enough, very good agreement is found between the prescribed K value and the J values found on several outer contours.

The crack growth analysis to be carried out here is somewhat similar to NEEDLEMAN's (1987) numerical study of the debonding of an inclusion from a metal matrix and the subsequent numerical study of crack growth at an interface (NEEDLEMAN, 1990). These studies were based on an interface potential that specifies a traction–separation relation similar to the dependence of interatomic forces on interatomic separation. Analogous computations for debonding and fiber pull-out in a metal–matrix composite have also been carried out recently by TVERGAARD (1990).

In the principle of virtual work the cohesive stresses σ and the corresponding separations δ (Fig. 1) give an additional contribution to the internal virtual work [see TVERGAARD (1990)]. Approximate solutions are obtained by a linear incremental method, based on using a finite-element approximation of the displacement fields in the incremental version of the principle of virtual work. The elements used are quadrilaterials each built-up of four triangular, linear-displacement elements. An example of the mesh used for the computations is shown in Fig. 2, where it is seen that a uniform mesh region with initial length B_0 in front of the initial crack tip is used to model crack growth. A special Rayleigh–Ritz finite-element method is used to control nodal displacements at the interface within the fracture process zone [see also TVERGAARD (1990)]. Prescribing increments of the edge displacements in terms of increments of the applied K is quite stable in the initial stage; but clearly this will not function in the later stage, where K has reached the steady-state value while the crack still grows. Also in the intermediate stage, where K generally grows for increasing crack length and would grow monotonically in a continuum formulation, the element discretization results in small oscillations of the K value during debonding. Thus, K even has transient decays, and it is necessary to be able to prescribe monotonic growth of the separation at the crack tip node. Such control of instabilities during debonding is effectively handled by the special Rayleigh–Ritz finite-element method.

As shown in Fig. 2 a uniform mesh region of length B_0 is used in front of the initial crack tip to model crack growth. The length of one square element in this uniform mesh region is denoted Δ_0, and thus $B_0 = 30\Delta_0$ for the mesh shown in Fig. 2. Most of the computations have been carried out for $\delta_c = 0.1\Delta_0$, with $\delta_1/\delta_t = 0.15$ and $\delta_2/\delta_t = 0.5$. A few computations with different values of the ratios δ_c/Δ_0, δ_1/δ_t or δ_2/δ_t have been carried out as well, to test the effect of these parameters. The radius of the outer boundary used for the mesh in Fig. 2 is specified by $A_0/\Delta_0 = 2000$.

The reference length R_0 defined by (1.9) scales with the extent of the plastic zone size, and therefore the ratio R_0/Δ_0 gives some indication of how well the mesh is able to resolve the stress and strain fields around the crack tip. As an example, for a material with $\sigma_Y/E = 0.003$, the work of separation (1.5) specified by $\hat{\sigma} = 3.5\sigma_Y$, $\delta_t/\Delta_0 = 0.1$, $\delta_1/\delta_t = 0.15$ and $\delta_2/\delta_t = 0.5$ results in $R_0/\Delta_0 = 9.18$, which gives a reasonable resolution of the near-tip fields and the fracture process zone. A better resolution is obtained by choosing A_0 smaller to δ_t; but this does not reduce the value of R_0 and thus the minimum values of Δ_0 needed to ensure small-scale yielding. Furthermore, B_0 must exceed the minimum crack growth length needed to reach steady-state conditions, and this length also scales with R_0. Thus, halving the values of Δ_0/δ_t gives a significant increase of the required mesh size, which strongly increases the need for computing time and storage. The mesh in Fig. 2 has been used for computations with relatively small values of $\hat{\sigma}/\sigma_Y$, whereas a larger mesh with $B_0 = 60\Delta_0$ and $A_0 = 9000\Delta_0$ was found necessary for larger values of $\hat{\sigma}/\sigma_Y$. The larger computations required about 75 CPU hours on an Apollo 10.000 computer.

A case has been tested with different values of Δ_0/δ_t. It has been found that doubling values of Δ_0/δ_t gives noticeably lower steady-state values of K_R^{ss}/K_0, while halving the value of Δ_0/δ gives slightly higher predictions of K_R^{ss}/K_0. Thus, the degree of mesh refinement chosen here gives a reasonable approximation of the accurate resistance curves.

3. PREDICTIONS

Computed crack resistance curves are presented in Fig. 3 for four values of $\hat{\sigma}/\sigma_Y$ with $N = 0.1$, $\sigma_Y/E = 0.003$ and $\nu = 0.3$. The calculations were continued until K_R ceases to increase, or almost ceases to increase, implying that steady-state conditions

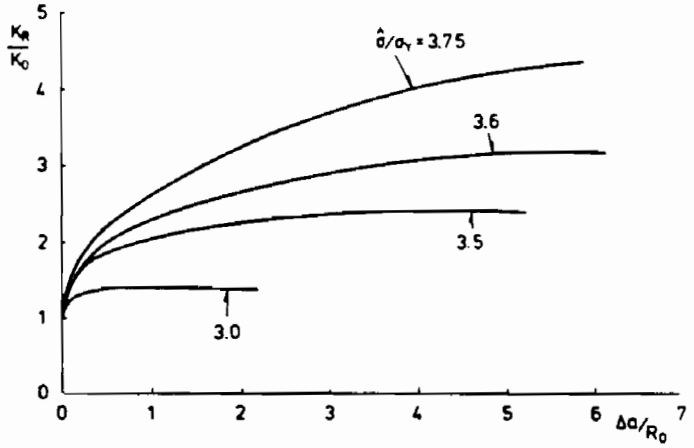

FIG. 3. Crack growth resistance curves with $\sigma_Y/E = 0.003$, $N = 0.1$, $\nu = 0.3$, $\delta_1/\delta_t = 0.15$ and $\delta_2/\delta_t = 0.5$.

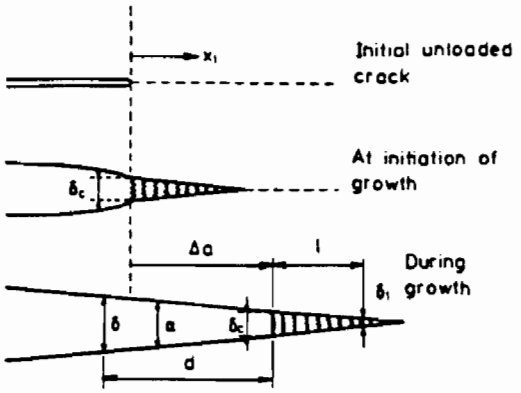

FIG. 4. Crack tip quantities.

were attained or almost attained. Several features of the near-tip field and the fracture process zone which will be discussed in detail are labeled in Fig. 4.

3.1. *Initiation of growth*

In Fig. 3 it can be seen that crack growth initiates at $K = K_0$ or, equivalently, at $\mathcal{G} = \Gamma_0$. Initiation of growth is associated with δ attaining δ_i at the original tip and the beginning of nonzero Δa, where Δa is measured from the end of the fracture process zone where all traction is lost. The initiation prediction can be understood by making use of the J-integral in (2.2) to connect the remote field to the fracture process zone (RICE, 1968). Under the assumption that the deformation theory of plasticity is a good model of the incremental flow theory prior to any crack growth, the J-integral can be shrunk from a remote contour surrounding the tip, where $J = \mathcal{G}$, to a contour along the fracture process zone giving

$$\mathcal{G} = \int_0^{\delta_i} \sigma(\delta)\, \mathrm{d}\delta, \tag{3.1}$$

where δ_i denotes the opening displacement at the original tip. Initiation of growth occurs when $\delta_i = \delta_i$ giving

$$\mathcal{G}_{ic} = \Gamma_0 \quad \text{or} \quad K_{ic} = K_0. \tag{3.2}$$

This result holds for finite-strain deformation theory. Its applicability to the incremental flow theory formulation used in the present calculations rests on the condition that stressing be proportional, or nearly proportional, in the plastic zone. Nonproportional stressing effects are all-important when crack growth occurs, excluding the use of this J-integral argument. However, the deformation theory model has been widely used and justified for stationary cracks. Its applicability here is corroborated by the fact that the present results in Fig. 3 confirm (3.2). Thus, the present model implies that the critical energy release rate at initiation depends on the

work of fracture, Γ_0, but is otherwise independent on other details of the fracture process and on σ_Y and N.

3.2. *Steady-state growth*

Let K_R^{ss} denote the limiting value of K_R attained as the cracks grows and approaches steady state. The nondimensional parameters which determine K_R^{ss}/K_0 are listed in (1.11). The dependence on $\hat{\sigma}/\sigma_Y$ and N is revealed in Fig. 5. The solid-line curves were computed with $\sigma_Y/E = 0.003$ and $\nu = 0.3$. A few calculations were also performed with $\sigma_Y/E = 0.006$ and $N = 0.1$, and these results are shown as a dashed-line curve close to the corresponding curve for $\sigma_Y/E = 0.003$ and $N = 0.1$. It is concluded that σ_Y/E has relatively little influence on K_R^{ss}/K_0, although σ_Y itself has a major influence through the dependence on $\hat{\sigma}/\sigma_Y$. The dependence on the shape of the traction–separation law as measured by δ_1/δ_c and δ_2/δ_c appears to be relatively weak as well. Computations for $\sigma_Y/E = 0.003$ and $N = 0.1$ were repeated using $\delta_c/\Delta_0 = 0.12$, $\delta_1/\delta_c = 0.125$ and $\delta_2/\delta_c = 0.25$, and these results are also seen to lie near the corresponding curve in Fig. 5 for $\delta_c/\Delta_0 = 0.10$, $\delta_1/\delta_c = 0.15$ and $\delta_2/\delta_c = 0.5$, the values used in all the other computations. The adjustment in δ_c/Δ_0 maintained a fixed ratio R_0/Δ_0 and thus comparable resolution in the two sets of computations.

The steady-state toughness is only slightly above the initiation toughness when $\hat{\sigma}/\sigma_Y$ is less than about 2.5. This is readily understood in terms of the traction which develops directly ahead of the crack tip in a fully developed plane strain plastic zone. For the line crack with no process zone in an elastic–perfectly plastic solid, the traction acting on the plane ahead of the tip in the plastic zone is (RICE *et al.*, 1980)

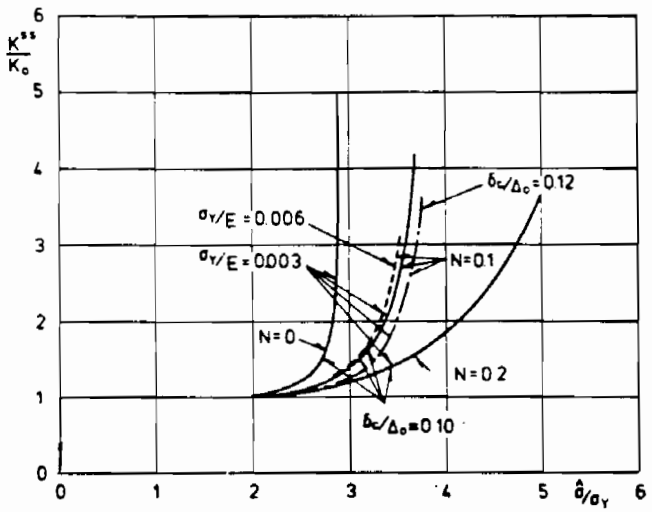

FIG. 5. Steady-state toughness as a function of $\hat{\sigma}/\sigma_Y$ for three levels of strain hardening exponent. The solid-line curves are with $\sigma_Y/E = 0.003$ and the curve (----) has $\sigma_Y/E = 0.006$, all with $\delta_1/\delta_c = 0.15$, $\delta_2/\delta_c = 0.5$ and $\nu = 0.3$. The curve (——) has $\sigma_Y/E = 0.003$ with $\delta_1/\delta_c = 0.125$, $\delta_2/\delta_c = 0.25$ and $\nu = 0.3$.

$$\sigma_{22} \cong \left(\frac{2+\pi}{\sqrt{3}}\right)\sigma_y = 2.97\sigma_y.$$

Hardening leads to even higher values of σ_{22}/σ_y ahead of the tip in a fully developed zone. Thus, if the peak traction required for the fracture process is less than about $2.5\sigma_y$, the crack initiates and advances without permitting a fully developed plastic zone to form. Plastic dissipation is then small compared to the work of the fracture process. It is important to appreciate that this is not precisely the same as saying that the plastic zone is negligible in size. The size of the plastic zone scales with R_0 in (1.9), which is proportional to Γ_0. The essential point is that plastic dissipation only becomes significant compared to Γ_0 when fully developed plastic zone can form.

Strain hardening as measured by N has a significant effect on steady-state toughness in Fig. 5. In the absence of strain hardening ($N = 0$), K_R^{ss}/K_0 increased dramatically as $\hat{\sigma}$ approaches $2.97\sigma_y$, since a traction greater than this cannot be achieved ahead of a crack in an elastic–perfectly plastic material. Without strain hardening and with $\hat{\sigma} > 2.97\sigma_y$, the model predicts that σ will never attain $\hat{\sigma}$ so that the opening displacement will lie in the range $0 < \delta < \delta_1$ in Fig. 1. The effective length of the fracture process zone will increase with increasing K, the crack tip will undergo increasing blunting, but crack advance will not take place. This feature is specific to the perfectly plastic limit and to the assumed model of the fracture process.

If the material strains hardens, K_R^{ss}/K_0 increases monotonically with $\hat{\sigma}/\sigma_y$. For fixed Γ_0, $\hat{\sigma}$ and σ_y, increasing N decreases K_R^{ss}, as can be seen in Fig. 5. Strain hardening increases the traction ahead of the tip and makes it easier to attain the peak stress $\hat{\sigma}$. For a similar reason, increasing σ_y decreases K_R^{ss} when Γ_0, $\hat{\sigma}$ and N are held fixed.

The length of the fracture process zone l, shown in Fig. 4, measures the distance between the point where all traction is lost and where the peak stress is first attained at $\delta = \delta_1$. This length varies little once crack growth has been initiated. For example, for $\hat{\sigma}/\sigma_y = 3.00$, $N = 0.1$ and $\sigma_y/E = 0.003$, $l/R_0 = 0.47$ when $\Delta a/R_0 = 0.30$ and $l/R_0 = 0.51$ when $\Delta a/R_0 = 2.08$. For $\hat{\sigma}/\sigma_y = 3.75$, $N = 0.1$ and $\sigma_y/E = 0.003$, $l/R_0 = 0.17$ when $\Delta a/R_0 = 0.54$ and $l/R_0 = 0.20$ when $\Delta a/R_0 = 5.8$. Moreover, l/R_0 was found to be virtually independent of σ_y/E, judging from a comparison of the calculations with $\sigma_y/E = 0.006$ with those for $\sigma_y/E = 0.003$. The steady-state value, l^{ss}/R_0, depends primarily on $\hat{\sigma}/\sigma_y$ and N, and this dependence is shown in Fig. 6.

After the crack has advanced a distance of about R_0, the opening profile in the fracture process zone, and in the region just behind the process zone, settles down to a fixed shape. This profile can be approximately characterized by a crack opening angle α, as illustrated in Fig. 4. The values of α in this plot are defined as $(\delta - \delta_c)/d$, where δ is the opening displacement a distance d behind the point where $\delta = \delta_c$. The steady-state value of $E\alpha/\sigma_y$ (the value attained after the largest crack advance computed) is plotted in Fig. 7. The parameter $E\alpha/\sigma_y$ has been used since, to a fairly good approximation, α is proportional to σ_y/E, as can be seen from the curve for $\sigma_y/E = 0.006$ and $N = 0.1$.

The characterization of the opening profile in the vicinity of the fracture process zone by a crack opening angle is only approximate. The following dependence of the steady-state opening angle on the choice of d for the case $N = 0.1$ and $\hat{\sigma}/\sigma_y = 3.6$ is typical: $\alpha = 4.05$, 3.50, 2.99 and 2.53° for $d/\Delta_0 = 3$, 6, 12 and 24, respectively.

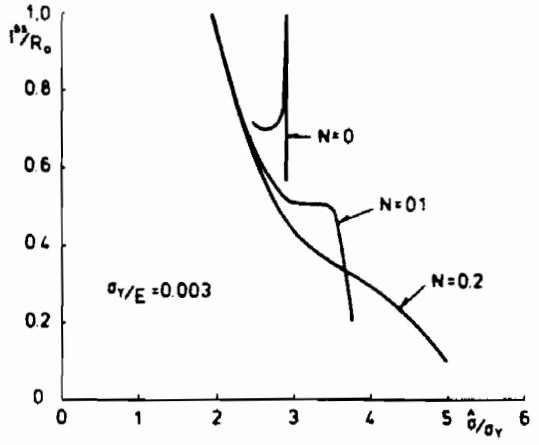

FIG. 6. Length of the fracture process zone in steady-state growth.

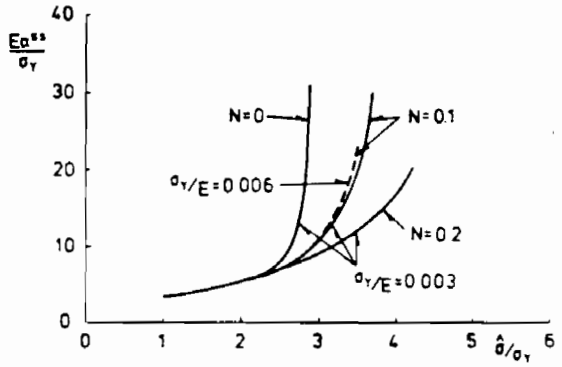

FIG. 7. Effective crack-opening angle in steady-state growth. See text for definition of angle.

Nevertheless, if the opening profile behind the advancing tip is invariant, then an effective opening angle based on a fixed choice of d can be used as a measure of the profile amplitude. This measure has been used to characterize the critical intensity of the near-tip field for growing cracks in numerical simulations (SHIH *et al.*, 1979; KANNINEN *et al.*, 1979).

4. INITIATION AND STEADY-STATE TOUGHNESSES FOR SOLIDS FAILING BY VOID GROWTH AND COALESCENCE

Many metals which fail by the void growth mechanism display a single fracture plane on which voids have grown and coalesced. This fracture process involves localization of plastic flow in a planar zone of essentially one void spacing in thickness, as evidenced by the fact that voids away from the planar zone display little or no

growth. The model developed below assumes a pre-existing population of roughly similar sized voids that give rise to a localized void sheet comprising the fracture process zone. The length l of this zone is assumed to be large compared to the void spacing. Thus the present model envisions a fracture process with many voids interacting on a plane ahead of the crack tip. The present model complements the RICE and JOHNSON (1970) model which assumes that the fracture process involves just one void interacting with the crack tip. Conditions determining the applicability of these two models will be discussed below. Neither the present model nor the Rice–Johnson model is applicable to the so-called zigzag mode of fracture which appears to involve shear localization on planes making an angle to the overall cracking plane.

We use the GURSON (1977) model for an elastic–plastic solid containing voids to predict the traction–displacement law associated with the fracture process zone. We will idealize the process by assuming that localization occurs in a layer of initial thickness λ. Later this thickness will be identified with the average void spacing, or some multiple of that spacing of order unity. The failure process is further idealized by assuming that voids are initially present with a void volume fraction f_0 or, equivalently, an area fraction f_0. The role of nucleation of the voids is discussed below.

The yield condition of the Gurson model is

$$\Phi(\sigma_e, \sigma_m, f) \equiv \left(\frac{\sigma_e}{\bar{\sigma}}\right)^2 + 2q_1 f \cosh\left(\frac{3\sigma_m}{2\bar{\sigma}}\right) - [1 + (q_1 f^2)^2] = 0, \tag{4.1}$$

where σ_e is the effective stress, $\sigma_m = \sigma_{kk}/3$ is the mean stress, $\bar{\sigma}$ is the current effective stress associated with the matrix, f is the current void volume fraction, and q_1 is the Tvergaard adjustment factor which will be taken to be 3/2 in the present study. The Gurson model was developed as a continuum model for dilatational plasticity, but the yield condition (4.1) was derived using a cell model to account for the interaction between voids. Thus, application of the model to compute the traction–displacement relation for the single plane of voids shown in Fig. 8 is fully consistent with its original derivation.

The traction–displacement relation is computed assuming the failing layer undergoes *uniaxial straining* in the direction normal to the plane (i.e. $\dot{\varepsilon}_{22} > 0$ with $\dot{\varepsilon}_{11} = \dot{\varepsilon}_{33} = 0$). Prior to attainment of the peak stress $\hat{\sigma}$, when localization becomes fully established, the constraint associated with uniaxial straining somewhat overestimates the actual constraint ahead of the crack tip. Once $\hat{\sigma}$ is attained, however, uniaxial straining conditions are fully in effect. ANDERSSON (1977) used these conditions in his model of void growth on the fracture plane ahead of a crack tip in plane strain.

The full set of equations for the Gurson model will not be listed here. They can be found in the original paper by Gurson or in the review article by TVERGAARD (1989). The true stress–logarithmic strain curve, $\bar{\sigma}$ vs $\bar{\varepsilon}$, characterizing the matrix is taken to be the same as used in the crack growth calculations, (1.6). The calculations reported below were carried out with $\nu = 0.3$ and various choices of σ_Y/E. These, together with N and f_0 which will be reported below, fully specify the model. Results are computed using a finite-strain formulation.

A set of traction–displacement curves is shown in Fig. 8 for four values of the initial

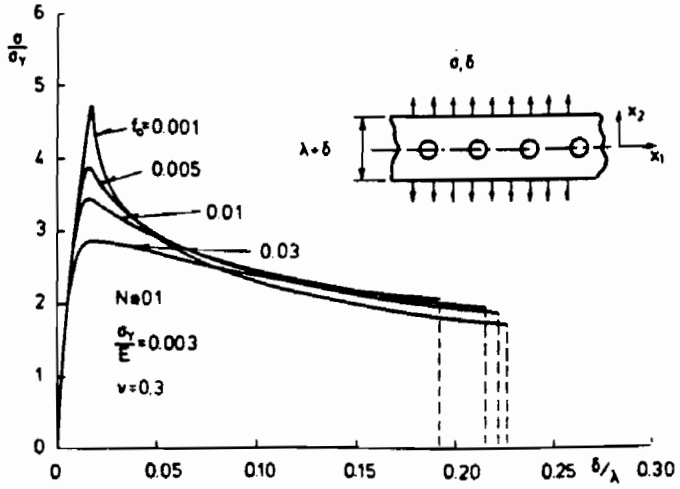

FIG. 8. Traction–separation curves predicted by the Gurson model for uniaxial straining.

void volume fraction f_0 with $N = 0.1$ and $\sigma_Y/E = 0.003$. In uniaxial straining, the true traction and the nominal traction are identical and here equal to σ; δ is the displacement of the top face of the layer relative to the bottom face. The initial thickness of the layer, λ, enters as a scaling length in all the results below. The curves have been terminated, with the traction dropped abruptly to zero, when the void volume fraction f reaches 0.2. This choice is somewhat arbitrary but is consistent with the observation [cf. discussion in TVERGAARD (1989)] that fine-scale localization involving necking down of the ligaments between voids sets in at a value of f between 0.15 and 0.25. This final stage of the coalescence process is not captured by the Gurson model. The abrupt termination of traction at $f = 0.2$ undoubtedly neglects some additional work of fracture. In the absence of a micromechanics model of this stage of the process, this simplification seems warranted, especially in the present exploratory application.

A plot of the normalized peak traction, $\hat{\sigma}/\sigma_Y$, as a function of f_0 is shown in Fig. 9(a) for three values of the strain hardening index. The work of fracture, $\Gamma_0 = \int \sigma \, d\delta$, is plotted as $W' = \Gamma_0/(\sigma_Y \lambda)$ in Fig. 9(b). While W' depends on N, it is relatively insensitive to f_0. Curves showing the influence of σ_Y/E on $\hat{\sigma}/\sigma_Y$ and W' are shown in Fig. 10. The values of $\hat{\sigma}/\sigma_Y$ and W' computed for the Gurson model will be used, together with the results of Section 3, to predict initiation and steady-state toughnesses as functions of N, f_0 and σ_Y/E. First, however, a remark will be made on how nucleation of voids can be expected to affect the fracture process.

Traction–displacement curves such as those in Fig. 8 were computed using a pre-existing void volume fraction f_0. In effect, nucleation is assumed to have occurred at zero stress. Very little void growth occurs by the point where the peak stress is attained. If no voids pre-exist but are nucleated by a volume fraction of particles, f_0, at a stress *below* the associated peak $\hat{\sigma}$ in Fig. 8, then the subsequent details of the traction–displacement curve will not differ greatly from the curve calculated with the voids present at the start (HUTCHINSON and TVERGAARD, 1989). In particular, the peak $\hat{\sigma}$

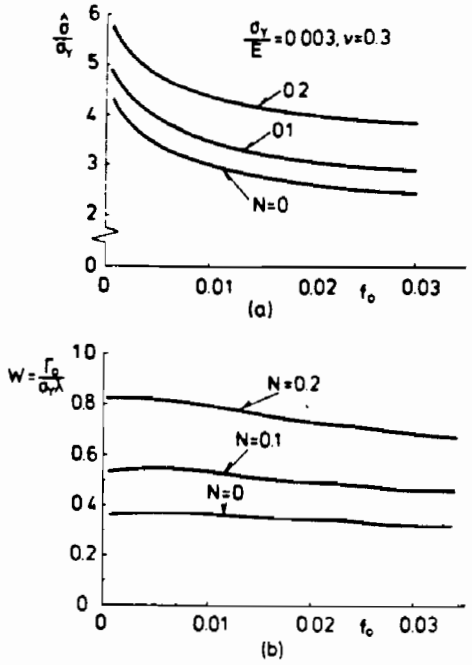

FIG. 9. Variations of the two most important fracture process parameters as a function of initial void volume fraction

will be only slightly greater and the work of fracture Γ_0 will be nearly the same. Thus, it can be argued that the predictions which follow are not very sensitive to the stress level at which the voids are nucleated, assuming that stress falls well *below* the peak stress associated with pre-existing voids measured by f_0. Nucleation stresses lying *above* the peak are expected to substantially enhance the toughness, as will be discussed below.

The shapes of the traction–displacement curves in Fig. 8 are somewhat different from those in Fig. 1 which were used to carry out the crack growth calculations. Nevertheless, the results reported in Section 3 indicate that the shape parameters have a relatively small influence and that the most important two parameters of the fracture processes are Γ_0 and $\hat{\sigma}$. We will use these parameters from Figs 9 and 10, together with the results for K_{I_c} and K_R^{ss} in Section 3, to study the dependence of these toughnesses on the basic material parameters.

As mentioned earlier, this approach requires that the length of the fracture process zone, l, be long compared to the thickness of the layer, λ, which itself is on the order of the void spacing. If the calculated value of λ/l turns out to be larger than 1.2, say, then the process zone modeled here involving multiple interacting voids will not occur. Instead, one would expect the fracture process to entail a single void interacting with the tip, as modeled by RICE and JOHNSON (1970). By (1.9),

$$\frac{\lambda}{l}=\frac{3\pi(1-\nu^2)}{W}\left(\frac{R_0}{l}\right)\frac{\sigma_Y}{E}. \tag{4.2}$$

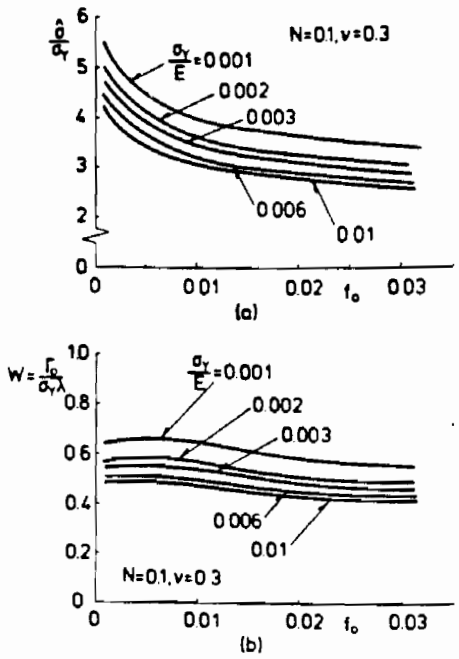

FIG. 10 Dependence of fracture process parameters on σ_Y/E.

Recall that l/R_0 never differs much from its steady-state value plotted in Fig. 6 and is essentially independent of σ_Y/E. Curves of λ/l as a function of f_0 are plotted in Fig. 11. These were determined using the steady-state results for l/R_0 and the dependence of $\hat{\sigma}/E$ and W' on f_0 in Figs 9 and 10. One concludes that the fracture process zone will involve many interacting voids as long as f_0 is not too small. The transition from the multiple-void regime to the single-void process zone is shown in Fig. 12, where the transition curves correspond to $\lambda/l = 0.5$. Results will be displayed below only when values of λ/l are less than 0.3.

From (3.2), the *initiation toughness* is given by K_0. Based on the present calculations

$$K_0 \equiv [E\Gamma_0(1-\nu^2)]^{1/2} = [E\sigma_Y\lambda(1-\nu^2)]^{1/2}W'^{1/2}, \tag{4.3}$$

where W' is plotted in Figs 9(b) and 10(b). Thus,

$$K_0 = \left[\frac{W'}{(1-\nu^2)}\right]^{1/2}(E\sigma_Y\lambda)^{1/2}. \tag{4.4}$$

The numerical coefficient $[W'/(1-\nu^2)]^{1/2}$ is between 0.7 and 1 and depends only weakly on f_0, N and σ_Y/E. This result is very similar to the initiation toughness prediction of RICE and JOHNSON (1970). They argue that initiation of growth takes place when the void nearest to the tip begins to coalesce with the tip. They estimate that this will happen when $\delta_t = cX_0$, where δ_t is the crack tip opening displacement, X_0 is the average spacing between voids, and c is a number which depends weakly on f_0, varying

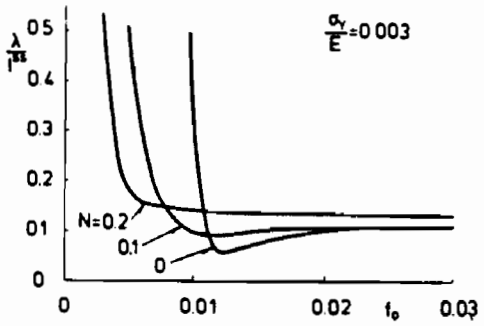

FIG. 11. Ratio of the thickness of the fracture process zone to its length as a function of initial void volume fraction. The thickness of the zone is approximately equal to the average void spacing.

from about 2 for $f_0 = 0.001$ to about 1 at $f = 0.05$. Using the small-scale yielding estimate, $\delta_t \cong 0.5(1-\nu^2)K^2/(E\sigma_Y)$, the Rice–Johnson prediction is

$$K_{Ic} = \left[\frac{2c}{(1-\nu^2)}\right]^{1/2} (E\sigma_Y X_0)^{1/2}. \tag{4.5}$$

If λ in the present model is identified with the averaging spacing between the voids, X_0, then (4.4) and (4.5) differ only in their numerical coefficients. The coefficient in K_{Ic} for the Rice–Johnson model is in the range of about 1.5–2 times that for the present model. Experimentally measured toughnesses generally do fall below the Rice–Johnson prediction (McMEEKING, 1977; GARRISON and MOODY, 1987), unless the materials are highly resistant to void nucleation. Accounting for small-scale voids between larger voids nucleated from inclusions reduces the theoretical toughness below (4.5) [e.g. ARAVAS and McMEEKING (1985) and NEEDLEMAN and TVERGAARD (1987)], a situation which may not be too different from that modeled in the present study.

There is nothing in either (4.4) or (4.5) which suggests that K_{Ic} could decrease with

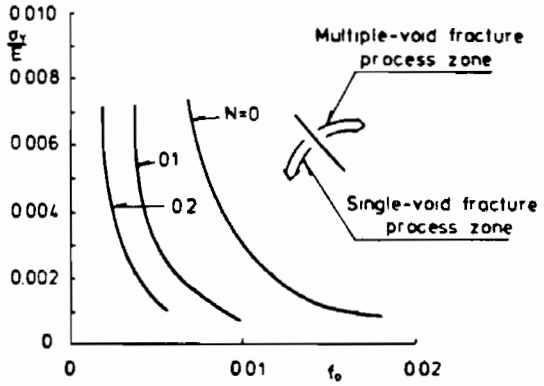

FIG. 12. Transition between regime in which the fracture process involves just one void interacting with the tip to regime involving multiple voids interacting ahead of the tip.

increasing σ_Y, a trend which has been reported for a number of structural alloys which are hardened [e.g. GARRISON and MOODY (1987)]. Even if the initial void volume fraction f_0 were to increase along with σ_Y, due, for example, to more void nucleation at the higher stress, the dependence of each prediction on f_0 is too weak to result in a drop in K_{Ii}. One possible explanation for a drop in initiation toughness with increasing σ_Y may be a transition from the single- to the multiple-void mechanism mapped in Fig. 12. Suppose, for example, that a combination of σ_Y and f_0 lies within the single-void regime, to the left of the transition line in Fig. 12. Then suppose that hardening the alloy derives the combination of σ_Y and f_0 across the transition into the regime where multiple voids comprise the fracture process. An increase in σ_Y increases the factor $(E\sigma_Y X_0)^{1/2}$ in each of (4.4) and (4.5), but crossing the transition results in a *drop* of a factor between 1.5 and 2 associated with the lower coefficient in (4.4) compared to (4.5). The net result would be a drop in K_{Ii}, assuming σ_Y was increased by less than about a factor of 2 in the process.

Steady-state toughness. K_R^{ss}, is determined using the fracture process parameters $\hat{\sigma}/\sigma_Y$ and W' in Figs 9 and 10 together with the plot of K_R^{ss}/K_0 in Fig. 5. By (4.3),

$$K_R^{ss}/[E\sigma_Y X_0/(1-\nu^2)]^{1/2} = (K_R^{ss}/K_0)W'^{1/2} \tag{4.6}$$

and this is the ordinate in Fig. 13. Strain hardening reduces the sensitivity of the steady-state toughness to initial void volume fraction f_0. With no hardening ($N = 0$), the toughness is very large for $f_0 \leqslant 0.01$ and drops precipitously in the range $0.01 < f_0 < 0.015$. As seen in Fig. 9(a), this is the range in which $\hat{\sigma}$ drops below $2.97\sigma_Y$, which, as discussed earlier, is the largest value of traction which can be attained ahead of the crack in a nonhardening material. For f_0 greater than 0.02, K_R^{ss} rapidly approaches K_{Ii}. By contrast, when $N = 0.2$, values of f_0 as small as 0.001 result in a nondimensional steady-state toughness (4.6) of about 5 and this value falls off gradually with increasing f_0 to a K_{Ii} level which is higher than the corresponding value for $N = 0$ by a factor of about 2.

The effect of σ_Y/E on the fracture process variables, $\hat{\sigma}$ and Γ_0, is shown in Fig. 10. In Fig. 10(a), it can be seen that σ_Y/E has a very strong effect on the normalized peak stress of the fracture process, $\hat{\sigma}/\sigma_Y$. A strong effect is to be expected since the peak stress is associated with plastic flow localization, and higher stress to modulus levels tend to promote such instabilities. The absolute value of $\hat{\sigma}$ increases as σ_Y/E increases, but the relative value, $\hat{\sigma}/\sigma_Y$, decreases. There is also some dependence of the non-

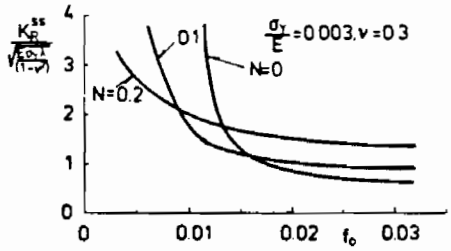

FIG. 13. Steady-state toughness as a function of initial void volume fraction.

dimensional work of fracture W' on σ_Y/E in Fig. 10(b), but this dependence is far less important than the reduction in $\hat{\sigma}/\sigma_Y$ in influencing steady-state toughness.

The effect of σ_Y/E on normalized steady-state toughness (4.6) is displayed in Fig. 14, where $N = 0.1$ and $\nu = 0.3$ for all curves. Recall that the effect of σ_Y/E on K_R^{ss}/K_0 in Section 3 is quite small compared to the effect of $\hat{\sigma}/\sigma_Y$ and N. The results in Fig. 14 were plotted using the curve in Fig. 5 for $N = 0.1$, neglecting any influence of σ_Y/E on the relation between K_R^{ss}/K_0 and $\hat{\sigma}/\sigma_Y$. By far the most important influence on steady-state toughness comes from the reduction of $\hat{\sigma}/\sigma_Y$ due to an increase in σ_Y/E, with a minor contribution due to the decrease in W'. At a given value of f_0, increasing σ_Y/E decreases the normalized steady-state toughness in Fig. 14, dramatically so in the range where the toughness is a strongly decreasing function of f_0. In the range of relatively small f_0, an increase in σ_Y will generally result in a *decrease* in K_R^{ss} itself. The present model therefore predicts that there is a range of material parameters such that the steady-state toughness, and presumably much of the resistance curve, will decrease as the initial flow stress is increased.

The role of nucleation was mentioned earlier where it was noted that, as long as voids are nucleated *below* the peak stress $\hat{\sigma}$ associated with f_0, the predictions of the model are expected to be relatively unaffected. If the nucleation stress is above $\hat{\sigma}$, the steady-state toughness is expected to be elevated in accord with the trends of Fig. 5. The fact that the present model has $K_{I_i} = K_0$, independent of $\hat{\sigma}$, suggests that the initiation toughness is unaffected by the nucleation stress. However, as the nucleation stress increases the ratio λ_i/l increases and the transition from the multiple-void regime to the single-void regime will take place. Then K_{I_i} will increase with increasing nucleation stress.

5. Qualitative Implications in Two Other Applications

5.1. *Toughness of an interface between similar solids*

Consider mode I crack growth along an interface between blocks of identical elastic–plastic solids where the blocks have been bonded by one of several possible methods, such as inertial welding, a thin adhesive layer, or thermal diffusion bonding. Let Γ_0 and $\hat{\sigma}$ characterize this interface bond, and let E, σ_Y and N characterize the

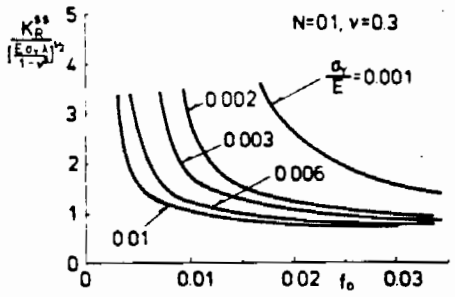

Fig. 14. Dependence of steady-state toughness on σ_Y/E.

properties of the material comprising the blocks. From the results of Section 3, one concludes that plastic dissipation in the blocks will only make a significant contribution to crack growth resistance if $\hat{\sigma}/\sigma_y$ is greater than about 2.5–3.5, depending on N. For smaller values of $\hat{\sigma}/\sigma_y$, there will be essentially no resistance curve behavior, and the effective toughness of the interface measured in units of energy/area will be Γ_0. These conclusions are predicted on the assumption that the scale of the fracture process is small compared to the size of the fracture process zone l predicted by the model, a condition which can be checked using the results of Section 3.

5.2. *On the steady-state toughness of dual-phase or reinforced solids*

Here a brief qualitative discussion is given of the implications of the model as to the role of plasticity in influencing steady-state toughness of dual-phase solids in which one phase is harder than the other. Crack bridging mechanisms are often present in dual-phase and reinforced solids. At issue is whether the steady-state toughness is due primarily to the work of fracture associated with the bridging mechanism and the small-scale fracture process or does dissipation in the surrounding plastic zone make a substantial contribution. The model suggests that plastic dissipation (other than that which is associated with the bridging/fracture process) will often be of minor consequence when the overall flow stress of the solid is as much as twice the flow stress of the softest phase. The argument is the following.

For simplicity of discussion, neglect strain hardening and let σ_0 denote the tensile flow stress of the softer phase. Let σ_y denote the overall tensile limit flow stress of the composite solid. The overall flow stress can be expressed as $\sigma_y = k\sigma_0$, where k is in the range 1.5–2, typically, for a well-strengthened composite solid. In applying the crack growth model of Section 3 to the composite solid, it is the overall flow stress σ_y which should be identified with the flow stress of the model, assuming that the plastic zone size, as measured by R_0, is large compared to the average spacing between the phase components. Thus, with reference to Fig. 5, it is seen that plastic dissipation (other than that associated with the bridging/fracture process) will only be important if $\hat{\sigma}\,\sigma_y = \hat{\sigma}\,(k\sigma_0)$ is larger than 2.5, or perhaps 3 if hardening is taken into account. If the reinforcement is such that k is from 1.5 to 2, the peak stress $\hat{\sigma}$ of the bridging/fracture process would have to exceed 3.75–5 times the flow stress of the soft phase σ_0 for plastic dissipation to make an important contribution to toughness. While it is possible under special conditions for the soft phase to sustain the high stresses implied by such large values of $\hat{\sigma}$, in general such high stresses cannot be expected to be achieved. Failure mechanisms such as phase boundary debonding, void nucleation at precipitates, and even cavitation will usually intervene before an overall stress of 3.75–5 times σ_0 can be attained.

ACKNOWLEDGEMENTS

The authors acknowledge the interest and encouragement of A. G. Evans. The work of JWH was supported in part by the National Science Foundation Grants NSF-MSM-88-12779, NSF-DMR-89-20490 and by the Division of Applied Sciences, Harvard University.

References

ANDERSSON, H. 1977 *J. Mech. Phys. Solids* **25**, 217.

ARAVAS, N. and MCMEEKING, R. M. 1985 *Int. J. Fracture* **29**, 21.

ESHELBY, J. D. 1970 In *Inelastic Behavior of Solids* (edited by M. F. KANNINEN *et al.*), p. 77. McGraw-Hill, New York.

GURSON, A. L. 1977 *J. Engng Mater. Technol.* **99**, 2.

GARRISON, W. M. and MOODY, N. R. 1987 *J. Phys. Chem. Solids* **48**, 1035.

HUTCHINSON, J. W. 1973 In *Numerical Solution of Nonlinear Structural Problems* (edited by R. F. HARTUNG), p. 17. ASME, New York.

HUTCHINSON, J. W. and TVERGAARD, V. 1989 In *Fracture Mechanics: Perspectives and Directions* (edited by R. P. WEI and R. P. GANGLOFF). ASTM-STP-1020, p. 62. Philadelphia, PA.

KANNINEN, M. F., RYBICKI, E. F., STONESIFER, R. B., BROCK D., ROSENFELD, A. R., MARSCHALL, C. W. and HAHN, G. T. 1979 In *Elastic–Plastic Fracture*, ASTM-STP-668, p. 121. Philadelphia, PA.

MCCLINTOCK, F. A. and IRWIN, G. R. 1965 In *Fracture Toughness Testing and Its Applications*, ASTM-STP-381, p. 84. Philadelphia, PA.

MCMEEKING, R. M. 1977 *J. Mech. Phys. Solids* **25**, 357.

NEEDLEMAN, A. 1987 *J. appl. Mech.* **54**, 525.

NEEDLEMAN, A. 1990 *J. Mech. Phys. Solids* **38**, 289.

NEEDLEMAN, A. and TVERGAARD, V. 1987 *J. Mech. Phys. Solids* **35**, 151.

RICE, J. R. 1968 In *Fracture, an Advanced Treatise* (edited by H. LIEBOWITZ), Vol. 2, p. 191. Academic Press, New York.

RICE, J. R. and JOHNSON, M. A. 1970 In *Inelastic Behavior of Solids* (edited by M. F. KANNINEN *et al.*), p. 641. McGraw-Hill, New York.

RICE, J. R. and SORENSEN, E. P. 1978 *J. Mech. Phys. Solids* **26**, 163.

RICE, J. R., DRUGAN, W. J. and SHAM, T.-L. 1980 In *Fracture Mechanics: Twelfth Conference*, ASTM-STP-700, p. 189. Philadelphia, PA.

SHAM, T.-L. 1983 In *Elastic–Plastic Fracture: Second Symposium, Vol. I—Inelastic Crack Analysis*, ASTM-STP-803, p. 52. Philadelphia, PA.

SHIH, C. F., LORENZI, H. G. and ANDREWS, W. R. 1979 In *Elastic–Plastic Fracture*, ASTM-STP-668, p. 65. Philadelphia, PA.

TVERGAARD, V. 1989 In *Advances in Applied Mechanics* 27 (edited by J. W. HUTCHINSON and T. Y. WU), p. 83. Academic Press, New York.

TVERGAARD, V. 1990 *Mater. Sci. Engng* **A125**, 203.